Hindawi
Advances in Civil Engineering
Volume 2020, Article ID 8850809, 10 pages
https://doi.org/10.1155/2020/8850809

Research Article

Bond Behavior between BFRP Rebar and Seawater Sea Sand Concrete

Chao Wu,[1] Bing-Chen Meng,[1] Xianfeng Cheng,[2] Asghar Habibnejad Korayem,[3] and Lik-Ho Tam[1]

[1]*School of Transportation Science and Engineering, Beihang University, 37 Xueyuan Road, Beijing 100191, China*
[2]*Hua Da Highway Engineering Consultant and Supervision Co., Ltd., Tuanjie East Road No. 21, Gaobeidian, Hebei 074000, China*
[3]*School of Civil Engineering, Iran University of Science and Technology, Narmak, Tehran, Iran*

Correspondence should be addressed to Lik-Ho Tam; leo_tam@buaa.edu.cn

Received 3 July 2020; Revised 12 September 2020; Accepted 15 September 2020; Published 25 September 2020

Academic Editor: Ayman S. Mosallam

Seawater sea sand concrete (SWSSC) is a promising alternative to ordinary concrete in terms of saving valuable natural resources of freshwater and river sand. Basalt fiber reinforced polymer (BFRP) rebars can be a good solution to corrosion of steel rebars in SWSSC. This paper presents an experimental study on the bond behavior between SWSSC and BFRP rebars through pullout testing. Concrete mixed with freshwater and river sand was also prepared for comparison with SWSSC. BFRP rebars with two different surface configurations were selected, that is, ribbed surface and sand-coated surface. Fly ash as a replacement of cement was also investigated in terms of its effect on bond behavior. Failure modes, bond-slip relationships, and bond strengths were reported and discussed in terms of the previously mentioned parameters. It was found that ribbed surface of BFRP rebar could achieve better mechanical interlocking with surrounding concrete. SWSSC could have comparative bond strength with BFRP rebar compared with ordinary concrete. However, using fly ash to replace cement is not recommended because it would significantly reduce concrete strength leading to much lower bond at the interface between SWSSC and BFRP rebar.

1. Introduction

Global concrete construction consumes great amount of freshwater and river sand, which represent valuable natural resources and are expected to become short by 2050 [1]. Concrete industry is thus facing great challenge with increasing concern of environmental and ecological issues. In addition, there is an increasing demand for coastal infrastructure due to rising sea levels. It will not be economical to use freshwater and river sand for concrete construction considering significant transportation cost. Motivated by these concerns, using seawater and sea sand to mix concrete (SWSSC) is a promising alternative to ordinary concrete [1–3].

It is reported that SWSSC can achieve similar mechanical properties to ordinary concrete mixed with freshwater and river sand [3, 4]. Partially replacing cement with geopolymer-based industrial waste, that is, slag and fly ash, could make concrete a green material as well as improving sustainability [4] and durability [5–7]. In addition, many studies have shown that use of fly ash has lots of advantages in waste recycling [6, 8] and improving concrete properties [9, 10]. However, one critical issue with SWSSC is that it cannot work with steel as either internal reinforcement or external constraining material. This is because SWSSC is rich in chloride, which may pose corrosion hazard to steel components [1, 11, 12]. In addition, seawater and sea sand may incur adverse effects on the workability and strength of SWSSC [13, 14].

The corrosion issue of steel reinforcements in SWSSC can be solved by using fiber reinforced polymer (FRP) rebars. FRP rebars have high specific strength and desirable corrosion resistance [15–17]. Many structural applications have shown that incorporation of FRP composites can be

cost-effective, in terms of construction speed, and improves structural durability [18]. Most of existing applications tend to use glass fiber FRP, carbon fiber FRP, and aramid fiber FRP [19]. Recently, another alternative is becoming available which is basalt fiber FRP or BFRP. Basalt fibers are produced by melting basalt at 1450–1500 degrees centigrade [20], and BFRP has excellent mechanical properties and chemical resistance [21, 22]. In addition, considering that BFRP is less toxic and harmless and more cost-effective compared with CFRP and GFRP [3, 21–23], BFRP has attracted increasing attention from construction industry. Therefore, reinforcing SWSSC using BFRP rebars can be a promising solution to environmental and corrosion issues with ordinary concrete structures.

Successful combination of SWSSC with BFRP rebars relies on the reliable bond behavior between the two [18], which determines mechanical performance of concrete components under bending, shear, torsion, and so on. [24]. The bond behavior is also critical to structural serviceability through limiting crack width and member deflections [25, 26]. Many researchers have carried out experimental and theoretical studies on bond behavior between FRP rebar and concrete [18, 24, 27–29]. It was found that the surface configuration of FRP rebars and concrete strength were the key factors affecting bonding mechanism [18, 27]. However, most of these studies focused on GFRP or CFRP rebars and ordinary concrete. Investigation on bond behavior between BFRP and SWSSC has been scarce in the literature.

In order to address this knowledge gap, this paper presents an experimental study on the bond behavior between BFRP and SWSSC through pullout testing. A total of 24 pullout tests were conducted considering effects of various parameters on the bond behavior. Two types of BFRP rebars were selected with different surface configurations, that is, ribbed surface or sand coated surface. SWSSC was compared with ordinary concrete mixed with freshwater and river sand. Cement was also partially replaced with fly ash in some specimens to see its effect on bond behavior. Failure modes, bond-slip curves, and bond strengths were reported. It was found that SWSSC could achieve comparative bond strength with BFRP rebar compared to ordinary concrete. However, replacing cement with fly ash is not desirable due to significant reduction in bond strength between SWSSC and BFRP rebars.

2. Experimental Program

2.1. Materials. Two types of BFRP rebars were selected with different surface preparation methods. Concrete mixed with seawater and sea sand was compared with that mixed with freshwater and river sand. Fly ash was also considered as an alternative material partially replacing cement to improve the greenness of concrete material.

2.1.1. Concrete. Two types of concrete materials are considered in this study. One is mixed with river sand and freshwater. The other is mixed with sea sand and seawater. Sea sand was transported from coast of Tianjin, the Bohai Sea, China. Seawater was artificially made by mixing NaCl powder in freshwater with a concentration of 3.5 wt. %. Similar NaCl solution has been frequently used as artificial seawater in the literature [30, 31]. Ordinary cement and fly ash were used as binder materials. Fly ash has been considered as an alternative binder material (30 wt. % replacement ratio) in order to evaluate how it may affect the strength of concrete and bonding behavior between concrete and BFRP rebar.

The particle size distributions of sea sand, river sand, and coarse aggregate were obtained through a sieving process according to ASTM C136 [32] as shown in Figure 1. The upper limit and lower limit of particle size distributions required by ASTM C33 [33] are also presented in Figure 1 for comparison purpose. It can be seen that the particle size distributions of sea sand, river sand, and coarse aggregate all satisfied the requirements by ASTM C33.

In addition, relative densities of coarse and fine aggregates were measured according to ASTM C127-15 [34] and ASTM C128-15 [35], respectively. Bulk densities of coarse and fine aggregates along with their moisture contents were measured according to ASTM C29/C29M-17a [36]. These measured physical properties of aggregates are listed in Table 1.

The mix proportions of the four scenarios for concrete are shown in Table 2. Regarding the name of each concrete mix, "O" means ordinary cement, and "F" refers to cement replaced with 30 wt.% fly ash. "R" stands for river sand and fresh water, while "S" means sea sand and seawater.

An HJW-60 single-horizontal concrete mixer was used for mixing the concrete materials. Slump of concrete was measured according to ASTM C143 [37]. Twenty-eight-day compressive strengths were tested using cubic specimens according to BS-1881-108 [38]. Concrete specimens were demolded after one day in the mold and then left in a water tank for curing until 28 days according to ASTM C192 [39]. Curing conditions of the water tank satisfied ASTM C511 [40]. For each mixing scenario in Table 2, at least three repeating tests were conducted for slump and strength results. The measured slumps and strengths of the four concrete scenarios are presented in Table 2.

It can be seen in Table 2 that, for the same binder material ("O" or "F"), seawater and sea sand in the mix may slightly reduce the compressive strength compared with the mix with freshwater and river sand. On the other hand, it seems replacing 30 wt.% cement with fly ash may significantly reduce the strength. Therefore, it can be said that when other parameters were unchanged, replacing 30 wt.% of cement with fly ash may significantly reduce the strength of concrete. Mixing concrete with seawater and sea sand may also negatively affect the concrete strength but only to a marginally extent.

2.1.2. BFRP Rebars. Two types of BFRP rebars were used in this study with different surface preparation methods as shown in Figure 2. Both rebars were manufactured through the pultrusion process with majority of the cross-section comprising continuous fibers. One rebar has a 0.65 mm

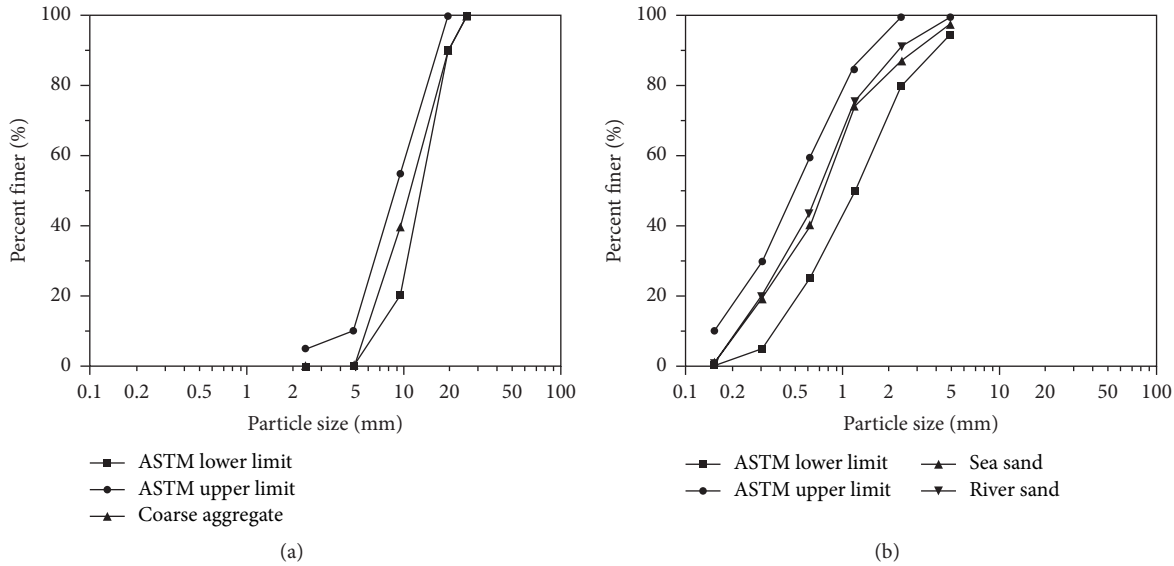

Figure 1: Particle size distributions of (a) coarse aggregate and (b) sea sand and river sand.

Table 1: Physical properties of aggregates used in this study.

Aggregates	Relative density (g/cm³)	Bulk density (g/cm³)	Fineness modulus	Moisture content (%)
Coarse aggregate	2.84	1.60	—	1.22
Sea sand	2.33	1.56	2.78	0.83
River sand	2.38	1.67	2.66	0.73

Table 2: Details of pullout testing groups and concrete mix design.

Group ID	Concrete mix								BFRP rebars
	Component (kg/m³)						Slump (mm)	Compressive strength (MPa)	
	Cement	Fly ash	Coarse aggregate	Fine aggregate	Water	NaCl			
OR-Rib OR-Sc	939	—	2842	1338	469	—	45	50.6	Ribbed Sand-coated
OS-Rib OS-Sc	939	—			453	16	42	47.4	Ribbed Sand-coated
FR-Rib FR-Sc	657	282			469	—	50	42.1	Ribbed Sand-coated
FS-Rib FS-Sc	657	282			453	16	48	40.9	Ribbed Sand-coated

thick sand coating on the surface in order to increase the bond with surrounding concrete (Figure 2(b)). The other rebar has a clear surface with regular ribs made through spiral winding. Fiber content of both rebars was measured through burn-off test according to ASTM D3171-15 [41]. The fiber content was measured as 91.09% by weight. Tensile strength and elastic modulus of both rebars were measured according to ASTM D638-14 [42]. The mechanical and physical properties of both BFRP rebars are listed in Table 3.

2.2. Specimens for Pullout Testing. Specimens were prepared for pullout testing to assess the bond behavior between BFRP rebar and concrete. Four specimens of concrete combined with two types of BFRP rebars yield eight testing groups, which are also shown in Table 2. For each testing group in Table 2, the first two letters represent the concrete. The second part refers to the type of BFRP rebar. "Rib" means rebar with ribbed surface and "Sc" stands for rebar with sand coated surface.

Details of the specimen for pullout testing are shown in Figure 3. The concrete was a cubic block with a dimension of 170 mm. BFRP rebar was embedded in the concrete block at the center of top surface with an embedded length of 90 mm, which was six times of rebar diameter. A debonding length of 80 mm was left at the end of BFRP rebar to reduce stress concentration when pulling rebar out of concrete block. The design of pullout specimen was according to ASTM D7913/

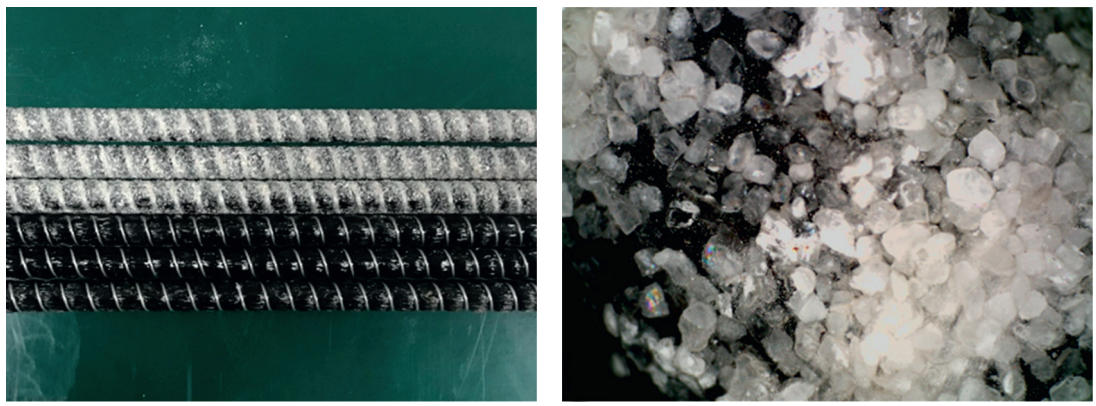

(a) (b)

Figure 2: (a) Two types of BFRP rebars and (b) microscopic image of sand coating.

Table 3: Mechanical and physical properties of BFRP bars.

Properties	Diameter (mm)	Tensile strength (MPa)	Elastic modulus (GPa)	Fiber content (%)	Fiber tensile strength (MPa)	Fiber elastic modulus (GPa)
Ribbed BFRP rebars	14.29	1351	43.08	91.09	4840	110
Sand-coated BFRP rebars	15.58		37.78			

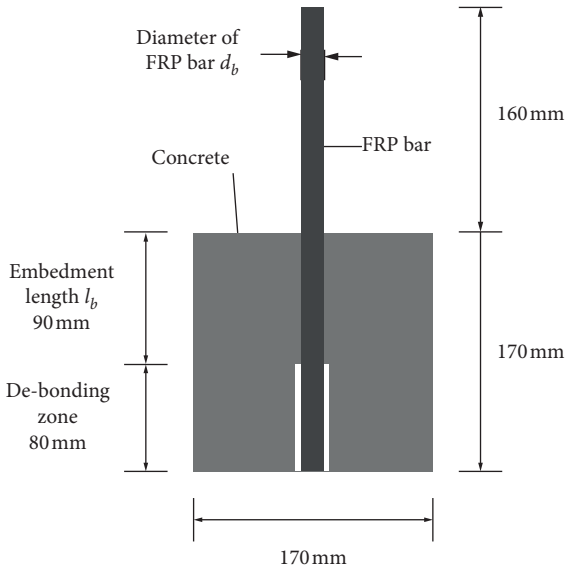

Figure 3: Specimen for pullout testing.

D7913M-14 [43]. For each testing group in Table 2, three identical specimens were prepared for repeating purpose. Therefore, a total of 24 specimens were tested.

When preparing pullout specimen, BFRP rebar was firstly cut into a specific length. Then, one end of rebar was inserted in a plastic tube of 80 mm long. The gaps between rebar and plastic tube were filled with silicone gel. After that, the rebar was installed vertically in the center of a cubic wooden box, which served as concrete mold. Concrete was then poured in the mold. When pouring concrete, a bubble level was used to insure rebar straightness. Concrete was demolded after one day. The plastic tube at the end of rebar was then removed creating debonding at the end of rebar (Figure 3).

2.3. Experimental Setup. The pullout test setup is shown in Figure 4. All tests were conducted using an MTS E45 universal testing machine with a capacity of 300 kN. A special fixture was manufactured in order to clamp the specimen when applying tensile load on rebar. A bottom steel plate of 32 mm thick was firstly clamped to the lower grip of machine. The pullout specimen was placed on the bottom plate and then covered by a top steel plate of 24 mm thick. The top and bottom steel plates were connected through four-threaded rods of 20 mm in diameter. The top steel plate had a center hole of 65 mm in diameter to allow rebar passing through. The rebar was clamped with the upper grip of machine. When the tensile force was applied on rebar, the top steel plate provided reaction forces on the concrete block. Two linear variable displacement transducers (LVDTs) were mounted on rebar to measure the slip of rebar relative to concrete block. The pullout test was conducted using displacement control at a speed of 1 mm/min until failure of specimen.

3. Experimental Results and Discussions

Each testing group was repeated for three times, and the experimental results were listed in Table 4 except three testing groups with ribbed rebar (i.e., OR-Rib, OS-Rib, and FR-Rib) for their data were significantly abnormal. The failure mode, bond-slip curve, and bond strength were discussed in this article.

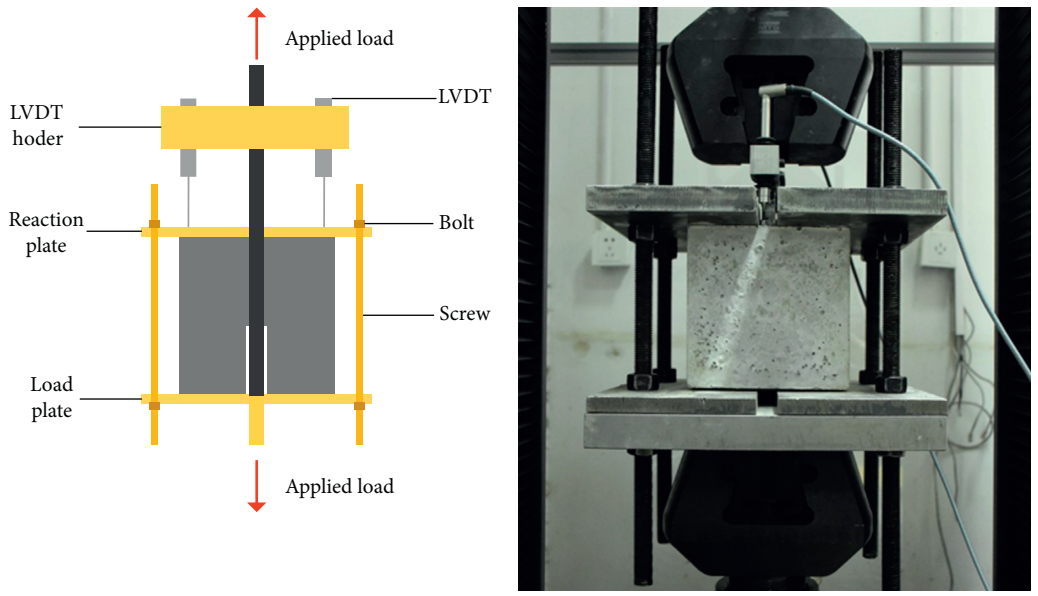

Figure 4: Setup and instrumentation of pullout testing.

Table 4: Experimental results of all pullout specimens.

Specimen ID	Bond strength (MPa)	Average bond strength (MPa)	Failure mode
OR-Rib-1	7.39	7.60	Concrete splitting
OR-Rib-2	7.80		Concrete splitting
OR-Sc-1	8.67	8.53	Pullout
OR-Sc-2	8.19		Concrete splitting
OR-Sc-3	8.72		Pullout
OS-Rib-1	11.75	10.71	Concrete splitting
OS-Rib-2	9.66		Concrete splitting
OS-Sc-1	9.82	9.20	Concrete splitting
OS-Sc-2	9.15		Pullout
OS-Sc-3	8.64		Pullout
FR-Rib-1	7.17	6.43	Concrete splitting
FR-Rib-2	5.68		Pullout
FR-Sc-1	5.89	6.19	Pullout
FR-Sc-2	6.10		Pullout
FR-Sc-3	6.58		Pullout
FS-Rib-1	10.92	9.91	Concrete splitting
FS-Rib-2	8.47		Concrete splitting
FS-Rib-3	10.33		Concrete splitting
FS-Sc-1	6.31	7.29	Pullout
FS-Sc-2	8.53		Pullout
FS-Sc-3	7.02		Pullout

3.1. Failure Modes. Two typical failure modes were observed as shown in Figure 5. For specimens with BFRP rebars with sand coating, the failure was rebar being pulled out from the concrete. The concrete block had no cracks on its surfaces as shown in Figure 5(a). Detailed examination of the rebar surface after failure is presented in Figure 5(b), which indicates that the failure was debonding at the interface between rebar and concrete. Traces of sand coating in Figure 5(b) suggest that sand particles slide on rebar surface when it was gradually pulled out from concrete.

For specimens with BFRP rebars of ribbed surface, the failure was much brittle with concrete block split into halves as shown in Figure 5(c). After the test, the cracked surface of concrete block was carefully examined in Figure 5(d). The interlocking mechanism between the rebar ribs and surrounding concrete was obvious from rebar indentations on concrete. Not much concrete debris was left on rebar surface indicating minimum slip between rebar and concrete before failure.

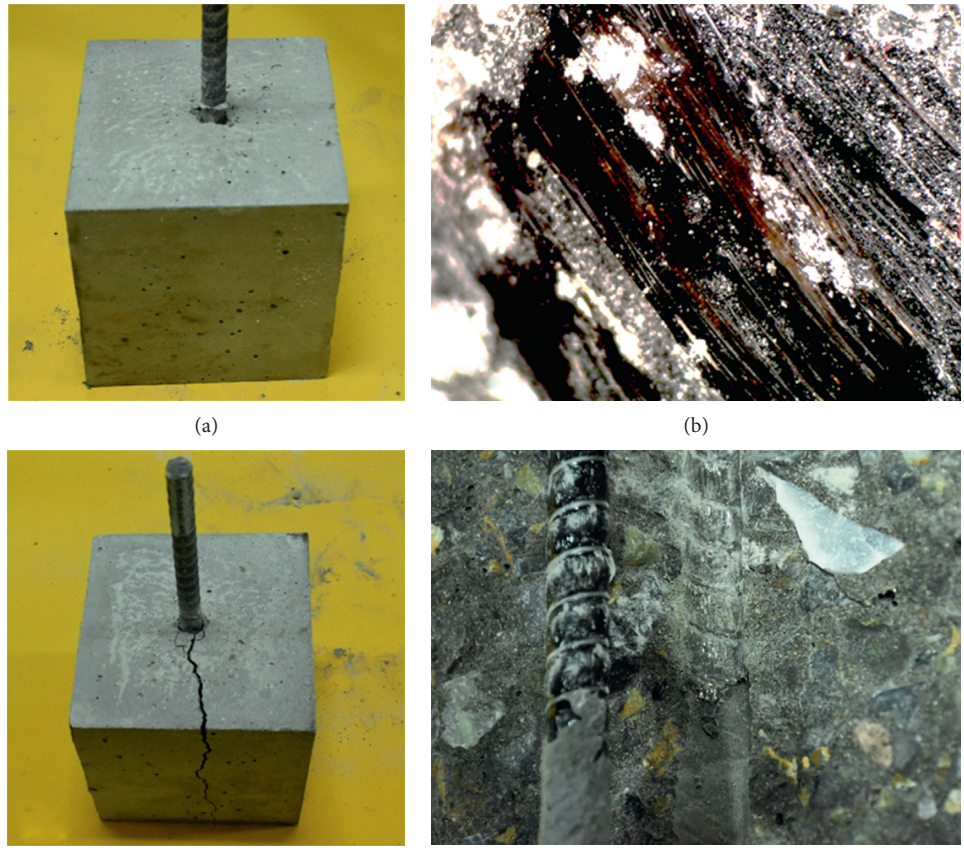

(a) (b)

(c) (d)

Figure 5: Typical failure modes of pullout specimens with (a) sand coated rebar and (c) rebar with ribs. The detailed examinations of surfaces of these two rebars are shown in (b) and (d), respectively.

3.2. Bond-Slip Curves. Typical bond-slip curves are chosen and plotted in Figures 6(a) and 6(b) for specimens with rebars of ribbed surface and rebars of sand coated surface, respectively. Bond stress τ_{av} at any stage of loading process can be calculated using the following equation:

$$\tau_{av} = \frac{F}{\pi d_b l_b}, \tag{1}$$

where F represents tensile load carried by the rebar, d_b is rebar diameter, and l_b refers to rebar embedment length which is 90 mm in this study.

The relative slip between rebar and concrete can be obtained from readings of the two LVDTs. It should be noted that the rebar extension should be excluded from LVDT readings due to the instrumentation setup as shown in Figure 4. Therefore, the interface slip can be determined by

$$\begin{aligned} s &= s_{av} - s_e, \\ s_e &= \frac{F l_a}{E A_b}, \end{aligned} \tag{2}$$

where s is relative slip between rebar and concrete at the interface, s_{av} is the average reading of two LVDTs, s_e is elastic extension of rebar with a segment length of l_a, and E and A_b are modulus and cross-section area of the rebar.

It can be seen in Figure 6 that all specimens showed a behavior with bond stress increased with slip-up to a peak point, after which the rebars were gradually pulled out with load dropping and slip increasing. It is also obvious in Figure 6 that specimens with ribbed rebar are more brittle than specimens with sand coated rebars. This is consistent with observations in failure modes in Figure 5. This is because the ribbed rebar has better mechanical interlocking with surrounding concrete than sand-coated rebar. Ribbed rebar specimens failed because of concrete splitting with little interface slip between ribbed rebar and surrounding concrete. Differently, sand-coated rebar failed because of interface slipping between rebar and concrete. The sand coating provides mechanical interlocking. With increase in tensile loading in the rebar, the coating fell off the surface and attached to the concrete hole. With the increase in interface slippage, friction force was developed which prevented sudden load drop.

In addition, specimens with ribbed rebar showed more scattering nature in the bond-slip curves than specimens with sand coated specimens. This is also related to their different failure modes. Specimens with ribbed rebar failed because of concrete splitting (Figure 5(c)), which may introduce significant uncertain factors such as concrete strength and cracking path. On the other hand, specimens with sand-coated rebar failed by interface

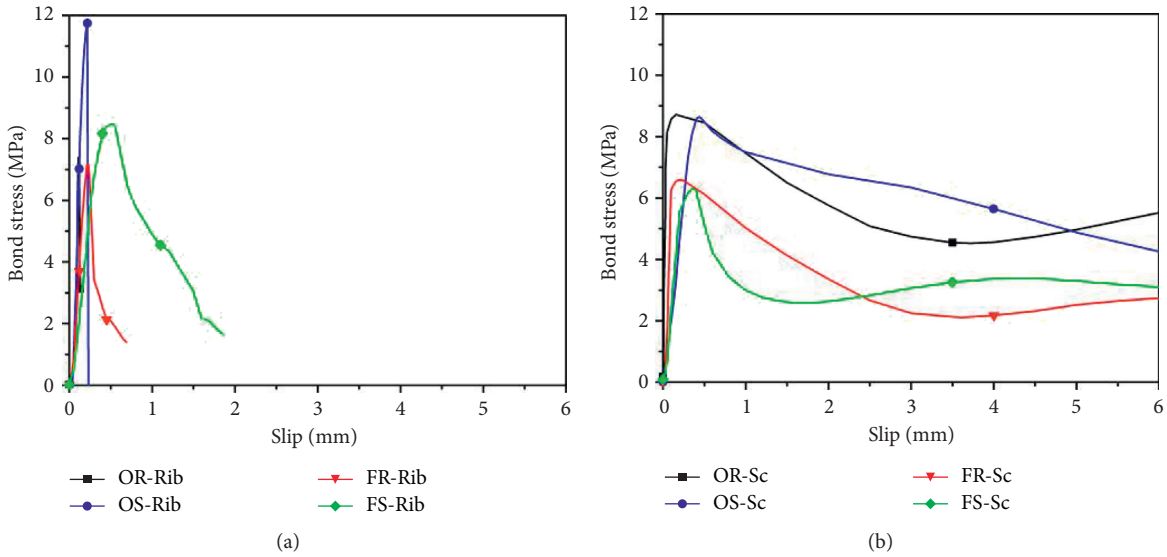

Figure 6: Typical bond-slip curves for specimens with (a) ribbed rebar and (b) sand coated rebar.

debonding (Figure 5(a)), which may yield more consistent results due to the controlled quality at the bonded interface.

3.3. Bond Strength. Peak stress of the bond-slip curve is defined as the bond strength of corresponding specimen. The bond strengths of all specimens are listed in Table 4. Since several identical specimens were repeated for each testing group in Table 2, their average strengths were plotted and compared in Figure 7.

Firstly, comparing specimens with ordinary cement and specimens with fly ash replacement, it is obvious that ordinary cement specimens always achieved higher bond strength than those with fly ash replacement. For example, OR-Rib strength is 7.60 MPa, which is higher than FR-Rib (6.43 MPa). Similar comparisons can be made for OR-Sc versus FR-Sc (8.53 MPa vs. 6.19 MPa), OS-Sc versus FS-Sc (9.20 MPa vs. 7.29 MPa), and OS-Rib versus FS-Rib (10.71 MPa vs. 9.91 MPa). This is reasonable because fly ash replacement may reduce the concrete strength as indicated in Table 2. Reduced concrete strength would lead to lower bond strength at the interface.

Secondly, comparing specimens with ribbed rebar and specimens with sand coated rebar, it is observed that most ribbed rebar specimens yielded greater bond strength than sand coated specimens. For example, comparisons can be made for OS-Rib versus OS-Sc (10.71 MPa vs. 9.20 MPa), FR-Rib versus FR-Sc (6.43 MPa vs. 6.19 MPa), and FS-Rib versus FS-Sc (9.91 MPa vs. 7.29 MPa). This can be associated with their different failure modes in Figure 5 of ribbed rebar specimens and sand coated rebar specimens. This indicates that ribbed surface may generate better mechanical interlocking with concrete than sand coated surface of BFRP rebar.

Thirdly, comparing specimens mixed with sea sand and seawater with specimens mixed with river sand and fresh water, it is interesting to notice that seawater specimens always exhibited greater strength than freshwater specimens. For example, this observation can be made when comparing OR-Rib versus OS-Rib (7.60 MPa vs. 10.71 MPa), OR-Sc versus OS-Sc (8.52 MPa vs. 9.20 MPa), FR-Rib versus FS-Rib (6.43 MPa vs. 9.91 MPa), and FR-Sc versus FS-Sc (6.19 MPa vs. 7.29 MPa). However, when looking at the compressive strength, concrete mixed with seawater is marginally weaker than concrete mixed with fresh water. Then, the question becomes why weaker concrete achieved stronger bond with BFRP rebar. This may be associated with the chemical reactions of BFRP rebar in the chloride environment. In chemistry, the following reactions will happen when basalt fiber is in contact with chloride solution [44]:

$$Fe^{2+} + Cl^{-} \longrightarrow [FeCl\,\text{complex}]^{-} \quad (3)$$

$$[FeCl\,\text{complex}]^{-} + OH^{-} \longrightarrow Fe(OH)_2 + Cl^{-} \quad (4)$$

$$Fe(OH)_2 + O_2 + H_2O \longrightarrow Fe(OH)_3 \longrightarrow Fe_2O_3 \cdot nH_2O \quad (5)$$

The previously mentioned reactions may improve the chemical bonding at the interface between BFRP rebar and surrounding concrete. In addition, formation of $Fe_2O_3.nH_2O$ may lead to geometry expansion of BFRP rebar whose diameter would increase. This geometry expansion of BFRP rebar is constrained by surrounding concrete and thus mechanical interaction at the interface may be enhanced.

In order to verify the abovementioned mechanism, basalt fibers were immersed in NaCl solution for 28 days as shown in Figure 8. Their diameters were measured before and after the immersion. It was found that the diameter of basalt fiber increased by 24.5%. Therefore, it can be said that the marginal drop in concrete strength due to mixing with sea sand and seawater can be significantly compensated in terms of interface bonding between BFRP and concrete. Two mechanisms

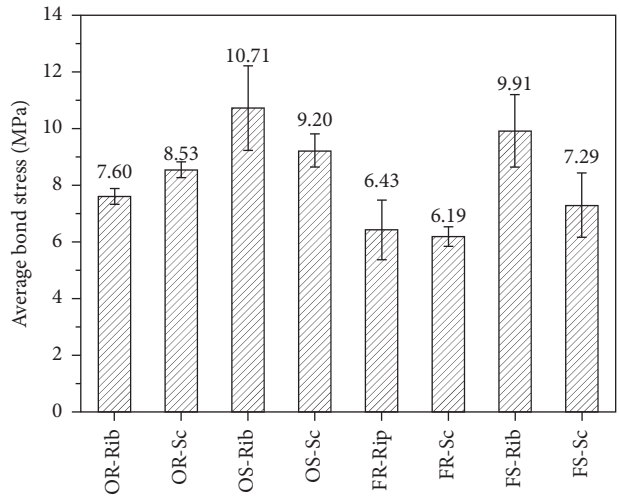

Figure 7: Comparison of bond strengths of all specimens.

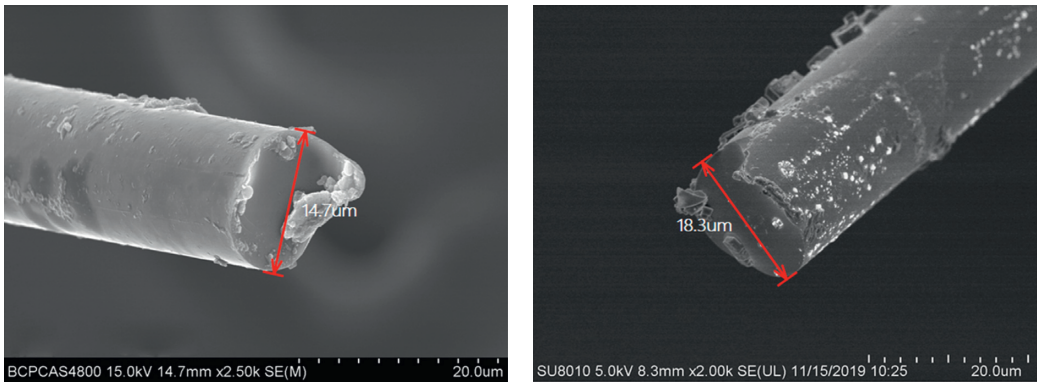

(a) (b)

Figure 8: Diameter of basalt fiber (a) before and (b) after immersion in sea water.

contributed to the improved bonding: the chemical interaction at the interface and the mechanical confinement due to geometry expansion of BFRP rebar.

4. Conclusions

This paper presents an experimental study on the bond behavior between BFRP rebar and concrete mixed with seawater and sea sand. Concrete mixed with freshwater and river sand was also prepared for comparison purpose. Fly ash was used to partially replace cement in some specimens to understand its effect on bond behavior. Pullout tests were conducted to quantify the bond behavior in terms of bond strength. Failure modes, bond-slip curves, and bond strength were reported, and the effects of various parameters on the bond strength were discussed. Based on the experimental results in this paper, the following conclusions can be drawn.

(1) Replacing cement with 30 wt.% fly ash may significantly reduce compressive strength of concrete (max by 20%). On the other hand, mixing concrete with seawater and sea sand may also reduce compressive strength of concrete, but the strength reduction was only marginal.

(2) Two failure modes were observed for pullout specimens. For specimens with ribbed rebar, they failed by concrete splitting. For specimens with sand coated rebar, the failure was interface debonding and no cracking was observed in concrete. Concrete splitting was more brittle than interface debonding.

(3) Specimens with ribbed rebar showed more scattering nature in the bond-slip curves due to significant uncertain factors such as concrete strength and cracking path introduced by concrete splitting. This is also related to their different failure modes.

(4) Replacing 30 wt.% cement with fly ash would result in lower bond strength between concrete and BFRP rebar, which was associated with the reduced strength of concrete. Ribbed surface seams more effective than sand-coated surface in terms of enhancement in bond strength. Ribs may provide a better mechanical interlocking with surrounding concrete than sand coating.

(5) Specimens with seawater sea sand concrete always showed higher bond strength than those with freshwater river sand concrete. The improvement in bond behavior was attributed to chemical reactions of basalt in chloride environment, which led to improved chemical interaction as well as enhanced mechanical interactions at the rebar-concrete interface due to geometry expansion of rebar. This is only based on the short-term measurement in the current study. How the chemical reaction and rebar expansion under seawater environment will affect the long-term bond behavior requires a more comprehensive future study.

(6) One interesting finding of the current study is that sand-coated rebar specimens have more ductile failure than the ribbed rebar specimens. Ribbed rebar specimens are failing near the split tension levels of concrete which means the concrete cannot take any more bond strength than was offered by rebar. This indicates that if the design bond strength can be compromised a little bit using sand-coated rebar, ductile failure is possible to be achieved.

This study proposes an environmentally friendly solution for construction and alleviates resource shortages and pollution to a certain extent. By proper design, it is recommended that seawater sea sand concrete (SWSSC) reinforced with BFRP rebars be a promising alternative to steel reinforced ordinary concrete, especially when the access to freshwater and river sand is limited.

Data Availability

The experimental data used to support the findings of this study are included within the article.

Conflicts of Interest

The authors declare that there are no conflicts of interest regarding the publication of this paper.

Acknowledgments

The first author acknowledges the financial support provided by the National Natural Science Foundation of China (51911530208 and 51978025) and Thousand Talents Plan (Young Professionals). The last author acknowledges the support from the National Natural Science Foundation of China (51808020) and the China Postdoctoral Science Foundation (2017M620015 and 2018T110029).

References

[1] F. Guo, S. Al-Saadi, R. K. Singh Raman, and X. L. Zhao, "Durability of fiber reinforced polymer (FRP) in simulated seawater sea sand concrete (SWSSC) environment," *Corrosion Science*, vol. 141, pp. 1–13, 2018.

[2] J. Teng, "Performance enhancement of structures through the use of fibre-reinforced polymer (FRP) composites," in *Proceedings of 23rd Australasian Conference on the Mechanics of Structures and Materials (ACMSM23)*, Lismore, Australia, December 2014.

[3] Z. Wang, X.-L. Zhao, G. Xian et al., "Long-term durability of basalt- and glass-fibre reinforced polymer (BFRP/GFRP) bars in seawater and sea sand concrete environment," *Construction and Building Materials*, vol. 139, pp. 467–489, 2017.

[4] T. U. Mohammed, H. Hamada, and T. Yamaji, "Performance of seawater-mixed concrete in the tidal environment," *Cement and Concrete Research*, vol. 34, no. 4, pp. 593–601, 2004.

[5] G. Li, "Properties of high-volume fly ash concrete incorporating nano-SiO_2," *Cement and Concrete Research*, vol. 34, no. 6, pp. 1043–1049, 2004.

[6] D. M. J. Sumajouw, D. Hardjito, S. E. Wallah, and B. V. Rangan, "Fly ash-based geopolymer concrete: study of slender reinforced columns," *Journal of Materials Science*, vol. 42, no. 9, pp. 3124–3130, 2007.

[7] T. Hashimoto and K. Torii, "The development of highly durable concrete using classified fine fly ash in Hokuriku district," *Journal of Advanced Concrete Technology*, vol. 11, no. 11, pp. 312–321, 2013.

[8] A. Matsuda, I. Maruyama, A. Meawad, S. Pareek, and Y. Araki, "Reaction, phases, and microstructure of fly ash-based alkali-activated materials," *Journal of Advanced Concrete Technology*, vol. 17, no. 3, pp. 93–101, 2019.

[9] R. Siddique, "Performance characteristics of high-volume class F fly ash concrete," *Cement and Concrete Research*, vol. 34, no. 3, pp. 487–493, 2004.

[10] T. M. Ha, S. Fukada, and K. Torii, "Effects of fly ash on mechanical properties of PC girder using reac-tive andesite aggregates," *Journal of Advanced Concrete Technology*, vol. 15, no. 10, pp. 579–594, 2017.

[11] J. Xiao, C. Qiang, A. Nanni, and K. Zhang, "Use of sea-sand and seawater in concrete construction: current status and future opportunities," *Construction and Building Materials*, vol. 155, pp. 1101–1111, 2017.

[12] K. Takewaka, T. Yamaguchi, and S. Maeda, "Simulation model for deterioration of concrete structures due to chloride attack," *Journal of Advanced Concrete Technology*, vol. 1, no. 2, pp. 139–146, 2003.

[13] S. K. Kaushik and S. Islam, "Suitability of sea water for mixing structural concrete exposed to a marine environment," *Cement and Concrete Composites*, vol. 17, no. 3, pp. 177–185, 1995.

[14] C. X. Xu, Z. W. Ou, J. L. Zhou, H. B. Chen, and Q. Chen, "Investigation on protectional ability on steel bar of compound corrosion inhibitor applied in seawater-and-sea sand concrete," *Applied Mechanics and Materials*, vol. 71–78, pp. 864–870, 2011.

[15] T. Uomoto, H. Mutsuyoshi, F. Katsuki, and S. Misra, "Use of fiber reinforced polymer composites as reinforcing material for concrete," *Journal of Materials in Civil Engineering*, vol. 14, no. 3, pp. 191–209, 2002.

[16] L. C. Hollaway, "A review of the present and future utilisation of FRP composites in the civil infrastructure with reference to their important in-service properties," *Construction and Building Materials*, vol. 24, no. 12, pp. 2419–2445, 2010.

[17] M. M. Rafi and A. Nadjai, "Experimental behaviour of carbon FRP reinforced concrete beams at ambient and elevated temperatures," *Journal of Advanced Concrete Technology*, vol. 6, no. 3, pp. 431–441, 2008.

[18] Z. Achillides and K. Pilakoutas, "Bond behavior of fiber reinforced polymer bars under direct pullout conditions," *Journal of Composites for Construction*, vol. 8, no. 2, pp. 173–181, 2004.

[19] Z. Q. Dong, G. Wu, and Y.-Q. Xu, "Bond and flexural behavior of sea sand concrete members reinforced with hybrid steel-composite bars presubjected to wet-dry cycles," *Journal of Composites for Construction*, vol. 21, no. 2, Article ID 04016095, 2016.

[20] V. Fiore, T. Scalici, G. Di Bella, and A. Valenza, "A review on basalt fibre and its composites," *Composites Part B: Engineering*, vol. 74, pp. 74–94, 2015.

[21] Z. Wang, X.-L. Zhao, G. Xian, G. Wu, R. K. Singh Raman, and S. Al-Saadi, "Durability study on interlaminar shear behaviour of basalt-, glass- and carbon-fibre reinforced polymer (B/G/CFRP) bars in seawater sea sand concrete environment," *Construction and Building Materials*, vol. 156, pp. 985–1004, 2017.

[22] Z. Wang, Z. Yang, Y. Yang, and G. Xian, "Flexural fatigue behavior of a pultruded basalt fiber reinforced epoxy plate subjected to elevated temperatures exposure," *Polymer Composites*, vol. 39, no. 5, pp. 1731–1741, 2018.

[23] Z. Lu, G. Xian, and H. Li, "Effects of elevated temperatures on the mechanical properties of basalt fibers and BFRP plates," *Construction and Building Materials*, vol. 127, pp. 1029–1036, 2016.

[24] E. Ahmed, E. El-Salakawy, and B. Benmokrane, "Bond stress-slip relationship and development length of FRP bars embedded in concrete," *HBCR Journal*, vol. 4, no. 3, pp. 1–17, 2008.

[25] M. Pecce, G. Manfredi, R. Realfonzo, and E. Cosenza, "Experimental and analytical evaluation of bond properties of GFRP bars," *Journal of Materials in Civil Engineering*, vol. 13, no. 4, pp. 282–290, 2001.

[26] J. Cairns and R. Abdullah, "An evaluation of bond pullout tests and their relevance to structural performance," *Structural Engineer*, vol. 73, no. 11, pp. 179–185, 1995.

[27] E. Cosenza, G. Manfredi, and R. Realfonzo, "Behavior and modeling of bond of FRP rebars to concrete," *Journal of Composites for Construction*, vol. 1, no. 2, pp. 40–51, 1997.

[28] A. Nanni, C. E. Bakis, and T. E. Boothby, "Test methods for FRP-concrete systems subjected to mechanical loads: state of the art review," *Journal of Reinforced Plastics and Composites*, vol. 14, no. 6, pp. 524–558, 1995.

[29] L. J. Malvar, "Bond stress-slip characteristics of FRP rebars," Technical Report TR-2013-SHR, Naval Facilities Engineering Service Center, Port Hueneme, CA, USA, 1994.

[30] M. E. Deniz and R. Karakuzu, "Seawater effect on impact behavior of glass-epoxy composite pipes," *Composites Part B: Engineering*, vol. 43, no. 3, pp. 1130–1138, 2012.

[31] H. Wang, Y. Huang, W. Zhang, and A. Ostendorf, "Investigation of multiple laser shock peening on the mechanical property and corrosion resistance of shipbuilding 5083Al alloy under a simulated seawater environment," *Applied Optics*, vol. 57, no. 22, pp. 6300–6308, 2018.

[32] ASTM International, *C136/C136M-19 Standard Test Method for Sieve Analysis of Fine and Coarse Aggregates*, ASTM International, West Conshohocken, PA, USA, 2019.

[33] ASTM International, *C33/C33M-18 Standard Specification for Concrete Aggregates*, ASTM International, West Conshohocken, PA, USA, 2018.

[34] ASTM International, *C127-15 Standard Test Method for Relative Density (Specific Gravity) and Absorption of Coarse Aggregate*, ASTM International, West Conshohocken, PA, USA, 2015.

[35] ASTM International, *C128-15 Standard Test Method for Relative Density (Specific Gravity) and Absorption of Fine Aggregate*, ASTM International, West Conshohocken, PA, USA, 2015.

[36] ASTM International, *C29/C29M-17a Standard Test Method for Bulk Density ("Unit Weight") and Voids in Aggregate*, ASTM International, West Conshohocken, PA, USA, 2017.

[37] ASTM International, *C143/C143M-15a Standard Test Method for Slump of Hydraulic-Cement Concrete*, ASTM International, West Conshohocken, PA, USA, 2015.

[38] British Standard Institution, *Testing Concrete: Method for Making Test Cubes from Fresh Concrete*, British Standards Institution, London, UK, 1983.

[39] ASTM International, *C192/C192M-19 Standard Practice for Making and Curing Concrete Test Specimens in the Laboratory*, ASTM International, West Conshohocken, PA, USA, 2019.

[40] ASTM International, *C511-19 Standard Specification for Mixing Rooms, Moist Cabinets, Moist Rooms, and Water Storage Tanks Used in the Testing of Hydraulic Cements and Concretes*, ASTM International, West Conshohocken, PA, USA, 2019.

[41] ASTM International, *D3171-15 Standard Test Methods for Constituent Content of Composite Materials*, ASTM International, West Conshohocken, PA, USA, 2015.

[42] ASTM International, *D638-14 Standard Test Method for Tensile Properties of Plastics*, ASTM International, West Conshohocken, PA, USA, 2014.

[43] ASTM International, *D7913/D7913M-14 Standard Test Method for Bond Strength of Fiber-Reinforced Polymer Matrix Composite Bars to Concrete by Pullout Testing*, ASTM International West, Conshohocken, PA, USA, 2020.

[44] B. Wei, H. Cao, and S. Song, "Degradation of basalt fibre and glass fibre/epoxy resin composites in seawater," *Corrosion Science*, vol. 53, no. 1, pp. 426–431, 2011.